Author/s:
Kim, CJ;Ercole, F;Goudeli, E;Bhangu, SK;Chen, J;Faria, M;Quinn, JF;Caruso, F

Title:
Engineering Programmable DNA Particles and Capsules Using Catechol-Functionalized DNA Block Copolymers

Date:
2022-08-23

Citation:
Kim, C. J., Ercole, F., Goudeli, E., Bhangu, S. K., Chen, J., Faria, M., Quinn, J. F. & Caruso, F. (2022). Engineering Programmable DNA Particles and Capsules Using Catechol-Functionalized DNA Block Copolymers. Chemistry of Materials, 34 (16), pp.7468-7480. https://doi.org/10.1021/acs.chemmater.2c01586.

Engineering Programmable DNA Particles and Capsules Using Catechol-Functionalized DNA Block Copolymers

Chan-Jin Kim,[†] Francesca Ercole,[§] Eirini Goudeli,[†] Sukhvir Kaur Bhangu,[†,‡] Jingqu Chen,[†] Matthew Faria,[†] John F. Quinn,[§,#] and Frank Caruso[,†]*

[†]Department of Chemical Engineering, The University of Melbourne, Parkville, Victoria 3010, Australia

[§]Drug Delivery, Disposition and Dynamics Theme, Monash Institute of Pharmaceutical Sciences, Monash University, Parkville, Victoria 3052, Australia

[‡]School of Science, RMIT University, Victoria 3001, Australia

[#]Department of Chemical Engineering, Faculty of Engineering, Monash University, Clayton, Victoria 3800, Australia

*Corresponding author. E-mail: fcaruso@unimelb.edu.au (F.C.)

ABSTRACT

DNA block copolymer (DBC) assemblies have attracted attention due to their tunable properties (e.g., programmability, high biocompatibility, efficient cellular uptake, and stability against enzymatic degradation), however, controlling the size of DNA block copolymer assemblies and preparing well-defined DNA-functionalized particle systems is challenging. Herein, we report the preparation of DBC-based particles and capsules with different sizes (i.e., from approximately 0.15 to 3.2 μm) and a narrow size distribution (i.e., polydispersity index < 0.2) through the assembly of catechol-functionalized DBC, DNA-*b*-poly(methyl methacrylate-*co*-2-methacryloylethyl dihydrocaffeate, with metal ions (e.g. Fe^{III}). This assembly process largely exploits the coordination bonding of the metal ions and phenolic (i.e., catechol) groups, forming metal–phenolic networks (MPNs). The DBC–Fe^{III} MPN capsules formed are stable under acidic, metal-chelating, and surfactant solutions due to the coexistence of metal coordination, hydrogen bonding, and hydrophobic interactions. The molecular recognition properties of the DNA strands enable tailorable interactions with small molecules and nanoparticles and are used to tune the permeability of the assembled capsules (>40% permeability decrease for 2000 kDa fluorescein isothiocyanate dextran compared with untreated capsules). The DBC–Fe^{III} MPN particles show efficient cellular uptake and endosomal escape capability, allowing the efficient delivery of small-interfering RNA for gene silencing (89% downregulation). The reported approach provides the rational design of a range of DNA-functionalized particles, which can potentially be applied in materials science and biomedical applications.

INTRODUCTION

Particle engineering, which involves the design and assembly of a range of particles, including hollow capsules,[1,2] surface-patterned colloids,[3] functional inorganic particles,[4] as well as self-

assembled polymeric structures[5] and biofunctional assemblies,[6] is of widespread scientific and industrial interest, spanning both biomedical and materials science applications.[7–9] Coating and thin-film technologies afford control of the surface and interfacial properties of particles, which can facilitate optimization for specific applications.[10] An example of a versatile coating technology is based on metal–phenolic networks (MPNs), which represents a robust and modular coating platform to control the surface and interfacial properties of various particle systems. MPN formation is driven by, in part, coordination interactions between metal ions and phenolic molecules, which typically comprise catechol and galloyl groups.[1,11] MPN films may be deposited on substrates of varying chemistry (e.g., inorganic, organic, and biological) irrespective of their dimensions (i.e., from nanometers to centimeters), and as such may be applied to prepare coated particles and capsules (i.e., when the solid core is removed) of varying sizes.[1] Although a variety of naturally occurring phenolic molecules such as tannic acid (TA) can be used to form MPNs, designing and synthesizing phenolic building blocks from functional macromolecules may improve the structural and functional diversity of resultant MPNs, thus broadening their potential applications.[12–14]

DNA block copolymers (DBCs), which are synthesized by covalent coupling of an oligonucleotide with a hydrophilic, hydrophobic, or amphiphilic polymer chain, have been extensively applied in the materials and biological sciences due to the programmability conferred by base sequence encoding, their high functional group density, and biocompatibility.[15–24] Moreover, DNA block copolymer assemblies exhibit a range of properties including high binding constants,[25,26] efficient cellular uptake,[26–28] and resistance to nuclease-catalyzed degradation,[26,29] which make them promising candidates for biological and medical applications (e.g., gene detection or delivery systems for anticancer drugs and therapeutic nucleic acids).[15,17] Additionally,

DNA block copolymer micelles containing dyes that emit in the second near-infrared region were fabricated for non-invasive imaging of brain tumors and a small-interfering RNA (siRNA)-based vesicle (siRNAsome) was developed for codelivery of therapeutic nucleic acids and drugs.[30,31] DNA block copolymers can self-assemble into spherical, vesicular, or low-dimensional structures (e.g., fibers, ribbons, and sheets), depending on the relative volume ratio between the hydrophilic and hydrophobic segments,[18,32,33] conjugated polymer type,[34–36] and hybridization between the complementary DNA strands.[37,38] However, DNA-functionalized particle systems such as spherical micelles and vesicles typically exhibit a broad size distribution, which is difficult to control.[5,34,35]

Herein, we report a versatile strategy for preparing DNA-functionalized particles and capsules using a DNA block copolymer composed of hydrophobic and catechol segments and featuring molecular recognition properties (DNA-*b*-poly(methyl methacrylate-*co*-2-methacryloylethyl dihydrocaffeate), DNA-*b*-poly(MMA-*co*-DHCAF)). The synthesized DNA block copolymer was used as a building block for preparing DNA-functional MPN particles and capsules that exhibit molecular recognition properties through the DNA segments. The size of the MPN particles and capsules was controlled from nanometers to micrometers and the MPN particles displayed a narrow size distribution depending on the selection of the template particles. These findings represent an advance over typical DNA block copolymer assemblies, for which it is challenging to achieve narrow size distributions. In addition, the DNA block copolymer-based MPNs were stable in strong acids, chelating environments, and surfactant solutions. This stability is likely due to the coexistence of multiple noncovalent interactions among the building blocks, including metal coordination, hydrogen bonding, and hydrophobic interactions. Molecular recognition via specific interactions between the complementary DNA strands was preserved on the MPN surface. In

addition, the permeability of the capsules could be tuned via hybridization between the complementary DNA sequences. The cellular uptake properties of the MPN particles were assessed as a function of DNA surface density, incubation time, and particle size and concentration. We also investigated the endosomal escape behavior, intracellular trafficking, and uptake mechanism of the particles and demonstrated successful delivery of a therapeutic nucleic acid. The present study demonstrates the rational design and fabrication of DNA-functionalized particles and capsules and highlights their potential in materials and biomedical science applications.

EXPERIMENTAL SECTION

Synthesis of DBC–Fe^{III} MPN Particles and Capsules. The DBC–Fe^{III} MPN particles were prepared as follows. Polystyrene (PS) template particles (0.147, 0.782, 1.01, 1.86, 2.86, and 3.25 μm in size; the size information is provided by the manufacturer) were dispersed in 3-(*N*-morpholino)propanesulfonic acid (MOPS) (pH 7.4; 100 μL, 50 mM) solution containing with NaCl (0.2 M). Then, a DNA1(fluorescein amidate, FAM)-*b*-poly(MMA_{40}-*co*-$DHCAF_{23}$) stock solution was added to the template dispersion and incubated overnight. An $FeCl_3 \cdot 6H_2O$ solution was subsequently added and mixed by vortexing for 2 min, followed by sonicating for 5 min. The final concentrations of the PS particles, DNA block copolymer chains, and Fe^{III} ions were 2.5 mg mL^{-1}, 3.75 μM, and 2 mM, respectively, in the 200 μL mixture. After incubating overnight, excess and unreacted materials were removed by pelleting the particles (2000 *g*, 5 min) and the supernatant was discarded. The DBC–Fe^{III} MPN-coated particles were washed thrice with water (500 μL) by repeated centrifugation (2000 *g*, 2 min) and redispersion in water (500 μL).

To prepare the DBC–Fe^{III} MPN capsules, the above coated particles were resuspended in water (50 μL), followed by the addition of tetrahydrofuran (THF) (1 mL) to remove the template

particles. After 1 h, the MPN capsules were pelleted through centrifugation (2000 *g*, 30 min) and washed with THF (500 μL) three times. At the final THF washing step, the capsules were once again pelleted through centrifugation before the supernatant was discarded. The resulting DBC–Fe^{III} MPN capsules were washed with water once and resuspended in water (300 μL).

Intracellular Uptake of DBC–Fe^{III} MPN Particles. The intracellular uptake of the DBC–Fe^{III} MPN particles was evaluated by flow cytometry and confocal laser scanning microscopy (CLSM). For flow cytometry, HeLa cells were seeded in a 24-well plate at 5×10^4 cells per well and then cultured in Dulbecco's Modified Eagle Medium (DMEM) with 10% fetal bovine serum (FBS) for 20 h at 37 °C in a 5% CO_2-humidified atmosphere to allow cellular adhesion on the plates. The DBC–Fe^{III} MPN particles (0.147, 0.782, and 3.25 μm) were added to the cells to achieve a final concentration of 10 nM, calculated based on DNA1(FAM), and then incubated for 24 h to examine cellular uptake. For the incubation time and concentration effect studies, 0.147 μm DBC–Fe^{III} MPN particles at a concentration equivalent to 10 nM DNA were incubated for 1–24 h and 0.147 μm DBC–Fe^{III} MPN particles at concentrations equivalent to 0.5–10 nM DNA were incubated for 24 h, respectively. Following incubation, the supernatant was discarded and the cells were washed thrice with Dulbecco's phosphate-buffered saline (DPBS; 500 μL). To facilitate cell detachment, trypsin solution (1×, 200 μL) was added, and the solution was maintained in an incubator (37 °C with 5% CO_2) for 5 min. For neutralization, DMEM solution (300 μL) was added and the detached cells were washed with DPBS (1 mL) three times through centrifugation (350 *g*, 5 min, 4 °C). The cells were dispersed in DPBS (400 μL) and cell association was analyzed by flow cytometry. Relative fluorescence intensity (RFI) refers to the fluorescence intensity of treated cells relative to the fluorescence intensity of untreated cells.

For the CLSM analysis, HeLa cells were seeded into 8-well Lab-Tek chambered coverglass slides (Thermo Fisher Scientific, Waltham, MA, USA) at a cell density of 4×10^4 cells per well and then cultured in DMEM with 10% FBS for 20 h at 37 °C in a 5% CO_2-humidified atmosphere to allow cellular adhesion on the plates. The prepared DBC–Fe^{III} MPN particles (10 nM) were added to the cells and then incubated for 24 h to evaluate cell association. Likewise, incubation for 1–24 h and particles at concentrations equivalent to 0.5–10 nM DNA were used for the specific experiment purposes. After incubation, the supernatant was removed and the cells were washed with DPBS (400 µL) twice. Cell fixation was performed by adding 4% paraformaldehyde (200 µL) for 20 min at room temperature, followed by washing with DPBS (400 µL) twice. The cell nuclei were dyed with Hoechst 33342 for 10 min at room temperature and the cell membranes were stained with wheat germ agglutinin–Alexa Fluor 594 conjugate (WGA594) for 5 min on ice. To investigate the endosomal escape of the DBC–Fe^{III} MPN particles (0.147 µm), the samples were gently washed twice with DPBS to remove excess MPN particles after incubation with HeLa cells for 24 h. LysoTracker Red was then added to the culture media to obtain a final concentration of 100 nM and incubated for 1 h following the supplier's protocol for endo/lysosome staining. Cells were gently washed three times with DPBS and fixed by adding 4% paraformaldehyde (200 µL) for 20 min at room temperature, followed by washing with DPBS (400 µL) twice. Cell nucleus staining with Hoechst 33342 was the performed under the aforementioned conditions. To monitor the cell association of the capsules, CLSM imaging was performed on a microscope equipped with a Plan Apo λ 60× 1.4 NA oil immersion objective, 405, 488, and 561 nm lasers, and 450/50, 525/50, and 595/50 bandpass emission filters. The images were processed using Fiji software.

Intracellular Trafficking by Confocal Microscopy. HeLa cells were seeded into 8-well Lab-Tek chambered coverglass slides at a cell density of 4×10^4 cells per well and then cultured in

DMEM with 10% FBS at 37 °C with 5% CO_2 for 20 h to allow cellular adhesion on the plates. The prepared 0.147 μm DBC–Fe^{III} MPN particles at a concentration equivalent to 10 nM DNA were added to the cells and then incubated for 12 or 24 h. The medium was then removed and the cells were washed twice with DPBS. Cell fixation was performed by adding 4% paraformaldehyde (200 μL) for 20 min at room temperature and subsequent washing with DPBS (400 μL) twice. Cells were then incubated in 0.2% Triton X-100 solution (200 μL) for 5 min for cell permeabilization, followed by washing three times with DPBS. To prevent nonspecific binding on the cell surface, the cells were incubated in 2.5% bovine serum albumin for 1 h. Samples were then incubated with rabbit anti-early endosome antigen 1 (EEA1) monoclonal antibody, rabbit anti-Ras-related protein 7 (Rab7) monoclonal antibody, or rat anti-lysosomal-associated membrane protein 1 (LAMP1) monoclonal antibody (2.5 μg mL^{-1}) overnight at 4 °C. The cells were washed three times with DPBS (400 μL) and incubated with goat anti-rabbit or goat anti-rat Alexa Fluor 647 conjugate antibody (10 μg mL^{-1}) for 1.5 h in the dark at room temperature. Thereafter, the cells were washed thrice with DPBS (400 μL) and the cell nucleus was stained with Hoechst 33342 as per above conditions. To monitor cell association of the capsules, CLSM imaging was performed on a microscope equipped with a Plan Apo λ 60× 1.4 NA oil immersion objective, 405, 488, and 640 nm lasers, and 450/50, 525/50, and 700/75 bandpass emission filters. The images were processed using Fiji software.

Intracellular Uptake Mechanism Study. HeLa cells were seeded in a 24-well plate at 5×10^4 cells per well and then cultured in DMEM with 10% FBS at 37 °C with 5% CO_2 for 20 h to allow cellular adhesion on the plates. Endocytosis inhibitors (5-(*N*-ethyl-*N*-isopropyl)amiloride (EIPA), pitstop 2, and filipin from *Streptomyces filipinensis* (*S. filipinensis*)) were added to the cells to achieve a final concentration of 20 μM. After 15 min incubation with the endocytosis inhibitors,

the prepared DBC–Fe^{III} MPN particles (0.147 μm) were added to the cells and then incubated for 4 h. After incubation, the supernatant was discarded, and the cells were washed with DPBS (500 μL) three times. To facilitate cell detachment, trypsin solution (1×, 200 μL) was added and the solution was maintained in an incubator (37 °C with 5% CO_2) for 5 min. For neutralization, DMEM solution (300 μL) was added and the detached cells were washed with DPBS (1 mL) thrice through centrifugation (350 *g*, 5 min, 4 °C). The cells were dispersed in DPBS (400 μL) and cell association was analyzed by flow cytometry.

Delivery of Therapeutic Oligonucleotides. PC3 cells expressing the firefly luciferase gene (PC3-Luc2) were seeded in a 96-well white plate (Costar 3917, Corning, MA, USA) at a density of 8000 cells per well in DMEM supplied with 10% FBS (100 μL) for 20 h. The free siRNA, siRNA–lipofectamine construct (siRNA complexed with lipofectamine RNAiMax transfection agent, Life Technologies; positive control), and siRNA-functionalized DBC–Fe^{III} MPN particles were incubated with cells in serum-free DMEM media with siRNA (final concentration of 10 nM) for 24 h. The serum-free media was removed and replaced with complete DMEM supplied with 10% FBS. After 48 and 96 h, the percentage of gene downregulation was evaluated using a ONE-Glo Luciferase Kit (Promega) following the manufacturer's protocol; luminescence readings were taken on an Infinite M200 microplate reader (Tecan, Switzerland).

Minimum Information Reporting in Bio-Nano Experimental Literature (MIRIBEL). The studies conducted herein, including material characterization, biological characterization, and experimental details, conform to the MIRIBEL reporting standard for bio–nano research,[39] and we include a companion checklist of these parameters in the Supporting Information.

RESULTS AND DISCUSSION

Design and Synthesis of DNA-*b*-poly(MMA-*co*-DHCAF). A programmable MPN building block, catechol-functionalized DNA block copolymer (DNA-*b*-poly(MMA-*co*-DHCAF), was synthesized by coupling a carboxylic acid-terminated catechol-functionalized copolymer with amine-terminated DNA strands (Scheme 1). Protection strategies for the catechol moieties in the phenolic molecule were used to minimize side reactions of the aromatic hydroxyls.[12] Specifically, 3-(3,4-dihydroxyphenyl)propanoic acid (dihydrocaffeic acid, DHCA) was used as a source of catechol groups, and the hydroxyl groups were protected by iBoc (isobutyl carbonate) groups to yield DHCA carbonic anhydride, iBocDHCA. A catechol-functionalized monomer was subsequently obtained by coupling iBocDHCA to 2-hydroxyethyl methacrylate. The synthesized iBocDHCA and iBocDHCA methacrylate were characterized by NMR spectroscopy (Figures S1 and S2). The catechol-functionalized copolymer, poly(MMA_{40}-*co*-$iBocDHCA_{23}$)-S(C=S)Ph, having a carboxylic acid end group, was then synthesized via reversible addition–fragmentation chain transfer (RAFT) copolymerization of iBocDHCA methacrylate and methyl methacrylate in the presence of a carboxylic acid functional chain transfer agent 4-cyano-4-(thiobenzoylthio)pentanoic acid. The RAFT end group of the resulting copolymer was then removed to prevent unwanted side reactions from occurring during the subsequent cleavage step (Scheme 1a).[40] The synthesized polymers (i.e., poly(MMA_{40}-*co*-$iBocDHCA_{23}$)-S(C=S)Ph (M_n = 11,220 g mol^{-1})) and poly(MMA_{40}-*co*-$iBocDHCA_{23}$)-H (M_n = 11,200 g mol^{-1})) were characterized by NMR spectroscopy and gel permeation chromatography (Figures S3 and S4).

The DNA block copolymer was synthesized by coupling the carboxylic acid end group of poly(MMA_{40}-*co*-$iBocDHCA_{23}$) to the amine group at the 5′ end of the oligonucleotide DNA1(FAM) attached to controlled pore glass (CPG) beads (Scheme 1b). After allowing 24 h for the coupling reaction to proceed, the CPG beads were washed consecutively with *N*,*N*-

dimethylformamide, chloroform, and acetone to remove unreacted polymers. The CPG beads were then kept in concentrated ammonium hydroxide at 55 °C for 5 h to release the synthesized DNA block copolymers and unreacted DNA strands from the beads. It is important to note that the protected catechol groups (i.e., iBoc groups) in poly(MMA_{40}-*co*-iBocDHCA$_{23}$)-H are also deprotected during this procedure.[41] The synthesized DNA block copolymers were then purified and characterized by gel electrophoresis (Figure S5a). Specifically, DNA1(FAM)-*b*-poly(MMA_{40}-*co*-DHCAF$_{23}$) remained in the loading well due to the formation of assemblies in water at high concentration, whereas unconjugated free oligonucleotides moved down during gel electrophoresis. The melting transition curves of DNA1(FAM)-*b*-poly(MMA_{40}-*co*-DHCAF$_{23}$) were determined based on Förster resonance energy transfer (FRET) between FAM-labeled DNA block copolymers and Cy3-labeled complementary DNA strands (DNA1′$_{18}$(Cy3)), confirming that the purified DNA block copolymer effectively bound complementary DNA (Figure S5b). Detailed DNA sequences used in this study are provided in Table S1.

Scheme 1. Synthesis of (a) poly(MMA-*co*-DHCAF) and (b) DNA-*b*-poly(MMA-*co*-DHCAF). Green, Brown, and Violet Represent DNA, MMA, and DHCAF, Respectively. CTBPA, 4-Cyano-4-(Thiobenzoylthio)pentanoic Acid; AIBN, 2,2′-Azobis(2-Methylpropionitrile); HATU, Hexafluorophosphate Azabenzotriazole Tetramethyl Uronium; DIEA, *N*,*N*-Diisopropylethylamine.

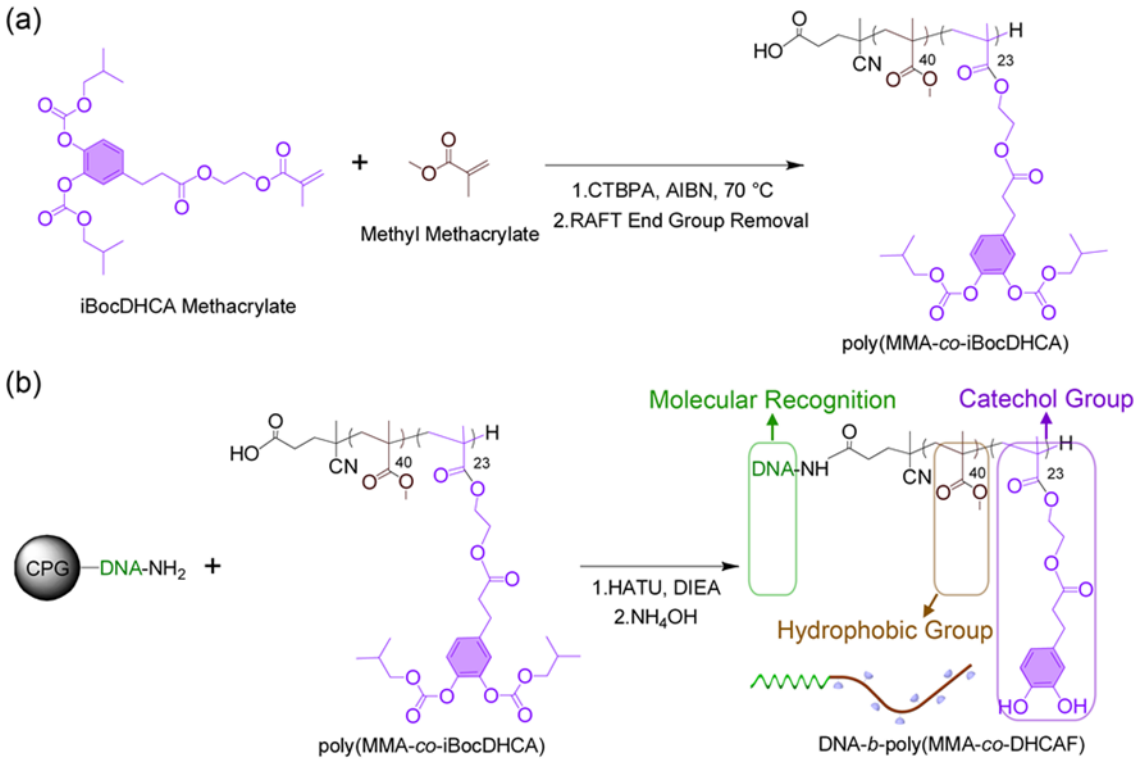

Fabrication of DNA-Functionalized MPN Particles and Capsules. To fabricate DNA-functionalized particles and capsules of different sizes with a narrow size distribution, the synthesized DNA block copolymers were used as the phenolic component in the MPN systems. DNA-*b*-poly(MMA-*co*-DHCAF) chains and Fe^{III} ions were assembled on sacrificial template particles (i.e., PS particles) to prepare DNA block copolymer–Fe^{III} (DBC–Fe^{III}) MPN particles and capsules (Figure 1a). PS particles were dispersed in MOPS buffer (pH 7.4), then mixed with DNA-*b*-poly(MMA-*co*-DHCAF) overnight to allow the adsorption of DNA block copolymer chains onto the particle surface. It is important to note that, as DNA-*b*-poly(MMA-*co*-DHCAF) is amphiphilic, the concentration used was less than the critical micelle concentration (determined to be 6.64 μM) (Figure S6), thus preventing formation of DNA block copolymer aggregates during MPN assembly. Addition of $FeCl_3 \cdot 6H_2O$ to the suspension resulted in the formation of bis- and tris-type coordination states between the catechol groups and Fe^{III} ions, where the bis-state is dominant.[13]

The final concentrations of the PS particles, DNA-*b*-poly(MMA-*co*-DHCAF), and Fe^{III} ions were 2.5 mg mL^{-1}, 3.75 μM, and 2 mM, respectively, in the mixture. We hypothesize that the coating process involves hydrogen bonding, hydrophobic interactions and metal coordination, as the DNA-*b*-poly(MMA-*co*-DHCAF) chain has hydrophobic, phenolic, and DNA bases which may each contribute to film formation. DBC–Fe^{III} MPN particles of different sizes were fabricated using PS template particles ranging from 0.147 ± 0.007 to 3.25 ± 0.08 μm in size and were characterized using scanning electron microscopy (SEM), transmission electron microscopy (TEM), and high-angle annular dark-field (HAADF) microscopy (Figures 1b, S7, S8, and S9). The microscopy analyses revealed that DBC–Fe^{III} MPN films were homogenously coated on the particle surface. Energy-dispersive X-ray spectroscopy (EDX) elemental mapping additionally revealed that C, N, O, P, and Fe were uniformly distributed throughout the DBC–Fe^{III} MPN particles, indicating that the films are composed of DNA block copolymers and Fe^{III} ions (Figure S9). Dynamic light scattering (DLS) data indicated that all prepared DBC–Fe^{III} MPN particles were well dispersed (polydispersity index < 0.26), and that the DBC–Fe^{III} MPN film coating on the particle surfaces resulted in a slight increase in apparent hydrodynamic diameter (Figure S10).

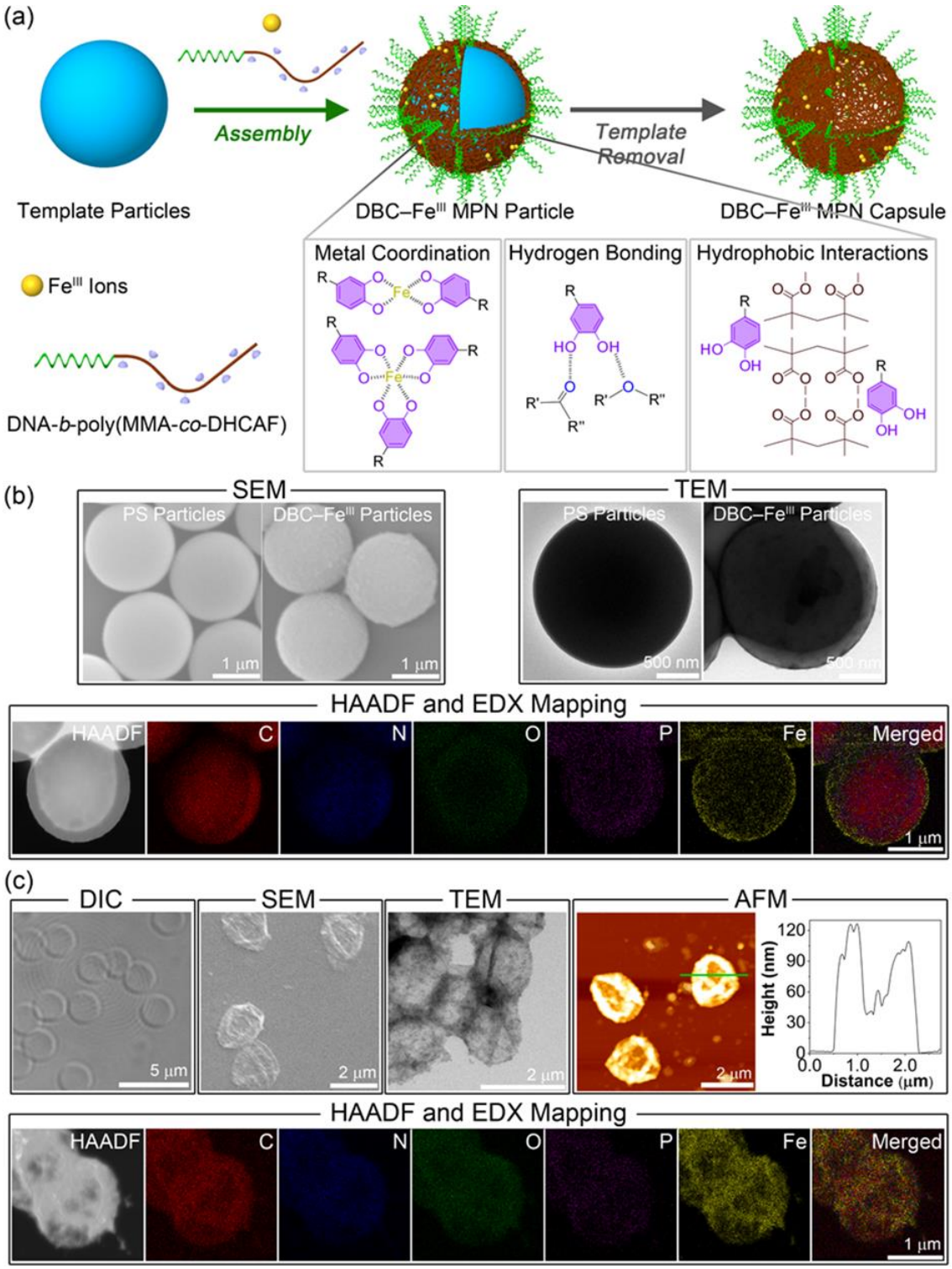

Figure 1. (a) Schematic illustration of the preparation of DBC–Fe^{III} MPN particles and capsules using DNA-*b*-poly(MMA-*co*-DHCAF) and Fe^{III} ions. Examples of the different interactions operating within the MPN systems are also depicted. Characterization of (b) DBC–Fe^{III} MPN

particles (1.86 ± 0.03 μm) using SEM, TEM, HAADF, and EDX mapping and (c) DBC–Fe^{III} MPN capsules (1.86 ± 0.03 μm) using DIC, SEM, TEM, AFM, HAADF, and EDX elemental mapping. The height versus distance profile of an MPN capsule plotted along the green line in the AFM image is also shown.

DBC–Fe^{III} MPN capsules were subsequently obtained by selectively dissolving the PS template particles using THF and characterized by differential interference contrast (DIC) microscopy, SEM, TEM, atomic force microscopy (AFM), HAADF microscopy, and EDX elemental mapping (Figures 1c and S11). The results indicate that the capsules were well dispersed and possessed folds and creases typical of air-dried capsules. The shell thicknesses of the DBC–Fe^{III} MPN capsules obtained using PS template particles of 1.86 and 3.25 μm in size were 19.3 ± 3.3 and 19.9 ± 2.1 nm, respectively, as determined from the minimum thickness of the capsules from the AFM measurements.

The stability of the DBC–Fe^{III} MPN interactions in various aqueous conditions was investigated using the DBC–Fe^{III} MPN capsules (Figure 2a). An acidic environment (i.e., 0.5 M HCl) is expected to revert coordination networks in MPNs to the mono-complex state.[12] A metal-chelating agent such as ethylenediaminetetraacetic acid (EDTA) can bind to the Fe^{III} ions in the MPN, resulting in the disruption of the MPN.[1] Tween 20 and urea can hinder hydrophobic and hydrogen bonding interactions, respectively, within the DBC–Fe^{III} MPN systems.[42,43] Interestingly, the DBC–Fe^{III} MPN capsules were stable in all the above solutions, which is likely due to the multiple binding modalities driving the assembly (i.e., metal coordination, hydrophobic interactions, and hydrogen bonding). Exposure to a low pH environment led to protonation of the DNA-*b*-poly(MMA-*co*-DHCAF) building blocks, resulting in a size contraction. The size contraction is likely due to a reduction in the electrostatic repulsion within the assembled complexes (Figure 2a).

Molecular dynamics simulations were performed to study the structural stability of the DBC–Fe^{III} MPN systems in various solvents (Figure 2b). To simplify the simulation calculation, we focused on the interactions between the poly(MMA-*co*-DHCAF) (BC) building blocks and Fe^{III} ions in BC–Fe^{III} MPN systems. The simulation studies confirmed that the BC–Fe^{III} MPN films assembled through the three interactions noted above (Figure 1a). Of these assembly interactions, metal coordination and hydrophobic interactions were determined to be the dominant forces (Figure 2c). The interactions between the poly(MMA-*co*-DHCAF) chains and Fe^{III} ions in BC–Fe^{III} MPN systems were monitored in different media (e.g., HCl, EDTA, and urea) and in vacuum (Figures S12–S14). Possible π–π interactions from the aromatic rings were quantified by calculating the intermolecular energy between the aromatic rings of the catechol groups among the six poly(MMA-*co*-DHCAF) strands. These interactions were negligible in all solvents and in vacuum compared to the metal coordination, and hydrophobic and hydrogen bonding interactions, indicating that poly(MMA-*co*-DHCAF) assembly is driven by the latter three interactions. The metal coordination interactions are more pronounced in HCl, while the BC–Fe^{III} MPN system interactions with HCl are weaker than with EDTA and urea, leading to reduced radius of gyration of the BC strands (Figure 2d), consistent with the experimental results (Figure 2a). These simulation results confirm that the assembled structures are stable in these harsh conditions due to the multiple assembly interactions, which is consistent with the experimental observations (Figure 2a).

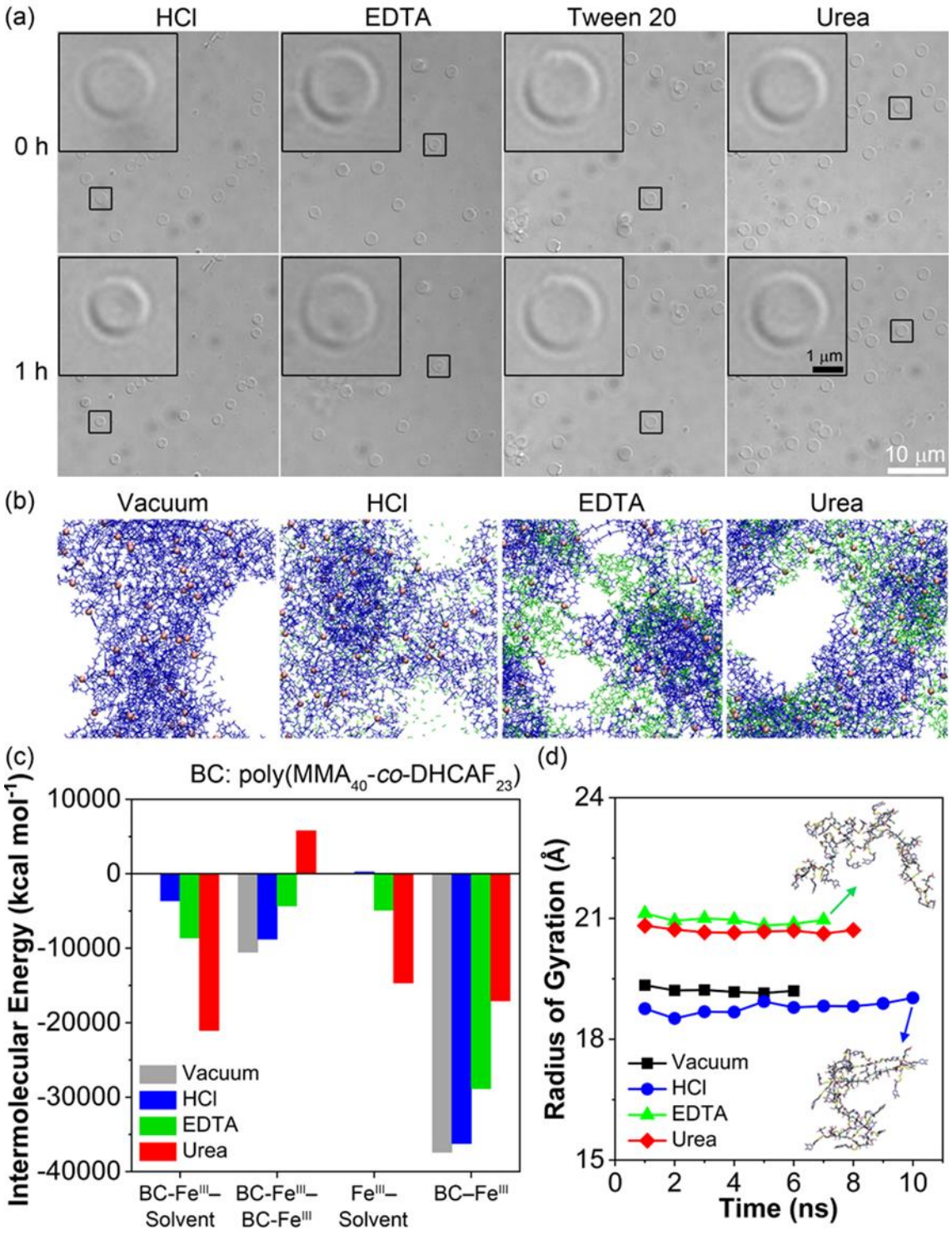

Figure 2. Structural stability of DBC–Fe^{III} MPN capsules (1.86 ± 0.03 μm) in different environments. (a) DIC images of the DBC–Fe^{III} MPN capsules before and after incubation for 1 h in 0.5 M HCl, or 100 mM EDTA, Tween 20, or urea. (b) Snapshots of the poly(MMA_{40}-*co*-

$DHCAF_{23}$) (BC) in vacuum, HCl, EDTA, and urea at 5 ns. The BC strands are shown as blue lines, Fe^{III} ions are shown as pink spheres and solvent molecules are depicted as green lines. (c) Average intermolecular energy between BC–Fe^{III} complex and solvent molecules, between BC–Fe^{III} and BC–Fe^{III}, between Fe^{III} ions and solvent, and between BC and Fe^{III} ions in vacuum, HCl, EDTA, and urea. (d) Average radius of gyration of the six BC strands in vacuum, HCl, EDTA, and urea. Insets show exemplarily the structure of the BC strands in EDTA and HCl.

Molecular Recognition Properties of DBC–Fe^{III} MPN Particles and Capsules. The molecular recognition properties of oligonucleotides have gained significant interest because they enable the fabrication of a diverse range of dynamic and complex nanostructures[31,44–46] and DNA-based sensors.[47,48] The sequence-specific binding interaction of DNA to the surface of the DBC–Fe^{III} MPN systems (i.e., particles and capsules) was confirmed by hybridization with DNA1′, a complementary sequence to DNA1 (Figure 3). The DBC–Fe^{III} MPN capsules have green fluorescence as the DNA block copolymer building block (i.e., DNA1(FAM)-*b*-poly(MMA_{40}-*co*-$DHCAF_{23}$)) has a fluorescein dye (FAM) at the 3′ end of the DNA strand. The resulting capsules were kept in MOPS (50 mM, pH 7.4) containing 0.6 M NaCl before further hybridization experiments, and the observed fluorescent ring structures were stable in this buffer, indicating the structural stability of these capsules at biological pH. Upon adding Cy3-labeled DNA strands ($DNA1'_{12}$(Cy3)) that are complementary to DNA1(FAM) over its entire 12 base length, the green fluorescence of the capsules was diminished due to FRET, while the red fluorescence from Cy3 was detected on the surface of capsules (Figure 3a, top panel). The DNA-directed interaction can be dynamically controlled using alternate DNA sequences, for example, through strand displacement switches.[44,49] For instance, $DNA1'_{12}$(Cy3) has a weak hybridization free energy (−11.29 kcal mol^{-1}) and can be removed from the capsules by the addition of $DNA1'_{18}$

(hybridization binding energy = −19.70 kcal mol^{-1}), which has six more complementary bases (i.e., is complementary to DNA1(FAM) over its entire 18 base length) (Table S2). The green and red fluorescence on the capsule surface were simultaneously recovered and diminished, respectively, indicating the exchange of DNA strands (Figures 3a and S15). Such a hybridization exchange approach is useful for molecular-level engineering of DNA-driven nanostructures for applications such as in programmable colloidal self-assembly,[50] optical switches,[51] and dynamic micromachines.[44] Furthermore, we demonstrate that these DBC–Fe^{III} MPN systems can be used as templates for self-assembly of functional nanoparticles through the specific binding affinity of oligonucleotides. Gold nanoparticles (AuNPs) were functionalized with thiol-modified DNA1 or DNA1′ by the salt aging method[52] and were denoted as AuNPs-DNA1 and AuNPs-DNA1′, respectively. The DBC–Fe^{III} MPN particles or capsules having DNA1 strands at the surfaces were mixed with AuNPs-DNA1′. This led to the coating of the particles or capsules with nanoparticles due to the sequence-specific interaction between DNA1 and DNA1′ (Figure 3b). To demonstrate the specificity of the interaction, when AuNPs-DNA1 were added to DBC–Fe^{III} MPN systems functionalized with DNA1, no significant attachment of nanoparticles was observed, as DNA1 does not bind to itself. (Figure 3b). These results demonstrate that the DBC–Fe^{III} MPN particles (and capsules) maintain the molecular recognition properties of DNA and may be used as templates for the self-assembly of functional molecules and nanoparticles.

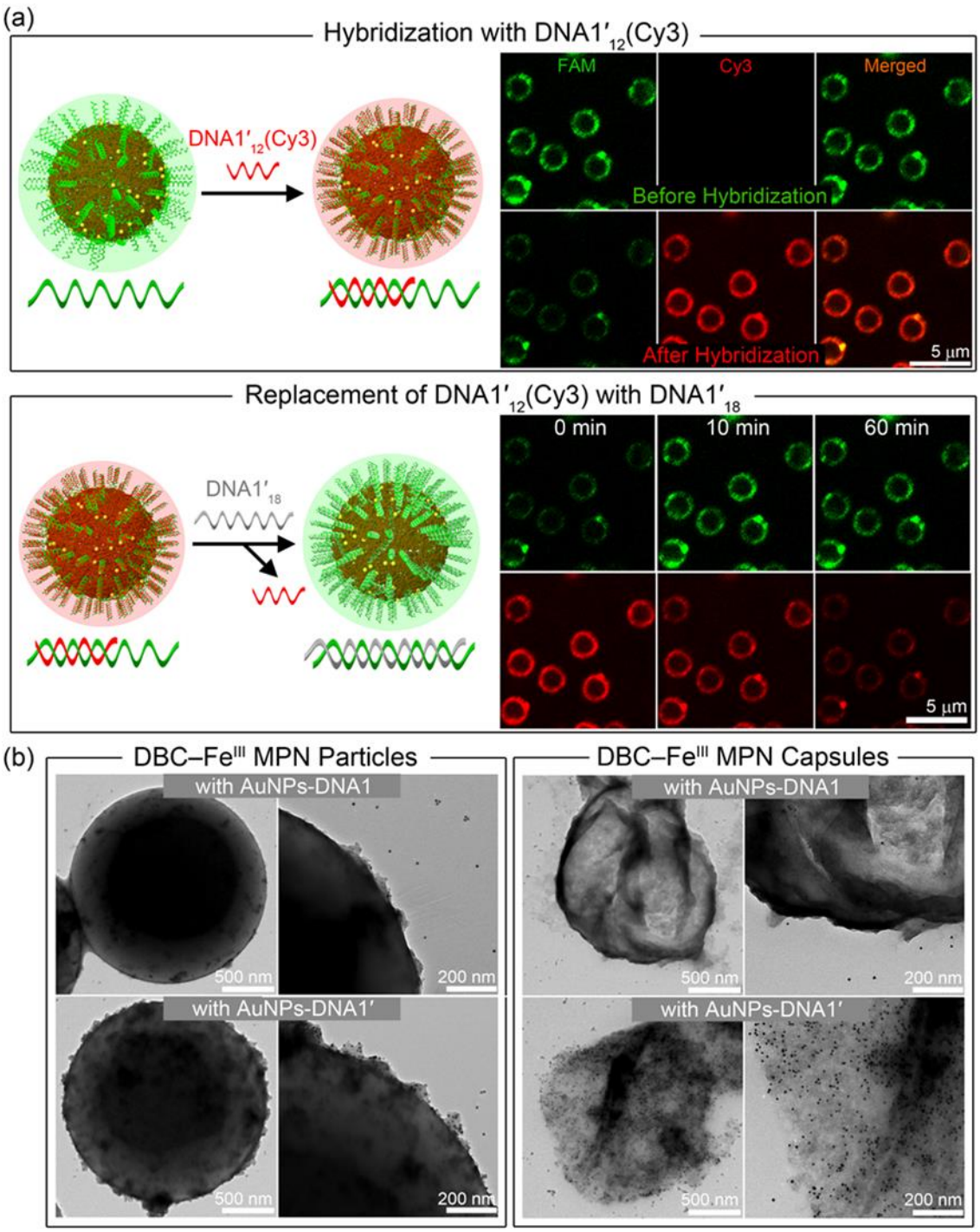

Figure 3. Molecular recognition properties of DBC–Fe^{III} MPN systems. (a) Attachment and detachment of dye molecules conjugated with complementary oligonucleotides from the surface of DBC–Fe^{III} MPN capsules (1.86 ± 0.03 μm) through different hybridization affinities with 12 base- (i.e., DNA1′$_{12}$(Cy3)) and 18 base- (i.e., DNA1′$_{18}$) matched complementary sequences. The

fluorescence intensity of FAM in DNA1(FAM) strands on the capsule surface was decreased upon adding DNA1′$_{12}$(Cy3) and was recovered upon adding DNA1′$_{18}$. (b) TEM images of DBC–Fe^{III} MPN particles (1.86 μm) and capsules (1.86 μm) mixed with AuNPs-DNA1 or AuNPs-DNA1′.

We subsequently investigated whether the permeability of the DBC–Fe^{III} MPN capsules could be controlled through hybridization of the DNA segment. The permeability of capsules was determined by incubating with fluorescein isothiocyanate (FITC)-dextran with molecular weights ranging from 4 to 2000 kDa. The untreated capsules were expected to be more permeable than those in which the DNA segment was hybridized with a connector strand composed of complementary and overhang sequences (DNA1′$_{12}$-A$_n$-DNA1′$_{12}$) (Figure 4a). The connector strand facilitates densification of the network structure by linking two DNA1 strands on the capsule surface. The lengths of the overhang sequences in the connector strands (DNA1′$_{12}$-A$_n$-DNA1′$_{12}$) were determined to be 3 and 9 nm for A$_{10}$ and A$_{30}$, respectively, as rod-like single-stranded oligonucleotides of 10 bases correspond to approximately 3 nm.[53] The diameters of gyration for the FITC-dextran molecules were generally much larger than the overhang sequences in the connector strands: 3.9 nm for 4 kDa, 8.4 nm for 20 kDa, 15.0 nm for 68 kDa, 28.1 nm for 250 kDa, 39.2 nm for 500 kDa, and 76.2 nm for 2000 kDa, as measured by Hanselmann and Burchard.[54,55] However, despite the obvious size difference between the connector strands and dextran, the permeability of the DBC–Fe^{III} MPN capsules to 4–68 kDa FITC-dextran could not be controlled via hybridization with connector strands, likely due to an insufficient density of DNA strands on the capsule surface. In contrast, the permeability of DBC–Fe^{III} MPN capsules to 250–2000 kDa FITC-dextran decreased upon adding connector strands to the capsules (Figures 4 and S16). Specifically, 81.9% and 76.2% of the native capsules were permeable to 250 and 2000 kDa FITC-dextran, respectively, whereas the capsules prehybridized with DNA1′$_{12}$-A$_{10}$-DNA1′$_{12}$

showed 43.6% and 33.1% permeability to 250 and 2000 kDa FITC-dextran, respectively. Moreover, the length of the overhang sequence (i.e., A_{10} and A_{30}) slightly influenced the permeability of the capsules, particularly toward 250 kDa FITC-dextran, with A_{10} and A_{30} yielding 43.6% and 71.9% permeability, respectively. This demonstrates the feasibility of controlling network structures on the MPN capsule surface via choice of the oligonucleotide length. Such tunable capsule permeability holds promise in diverse research areas, including nano/microreactors, separations, sensing, and delivery systems.[13,56–59]

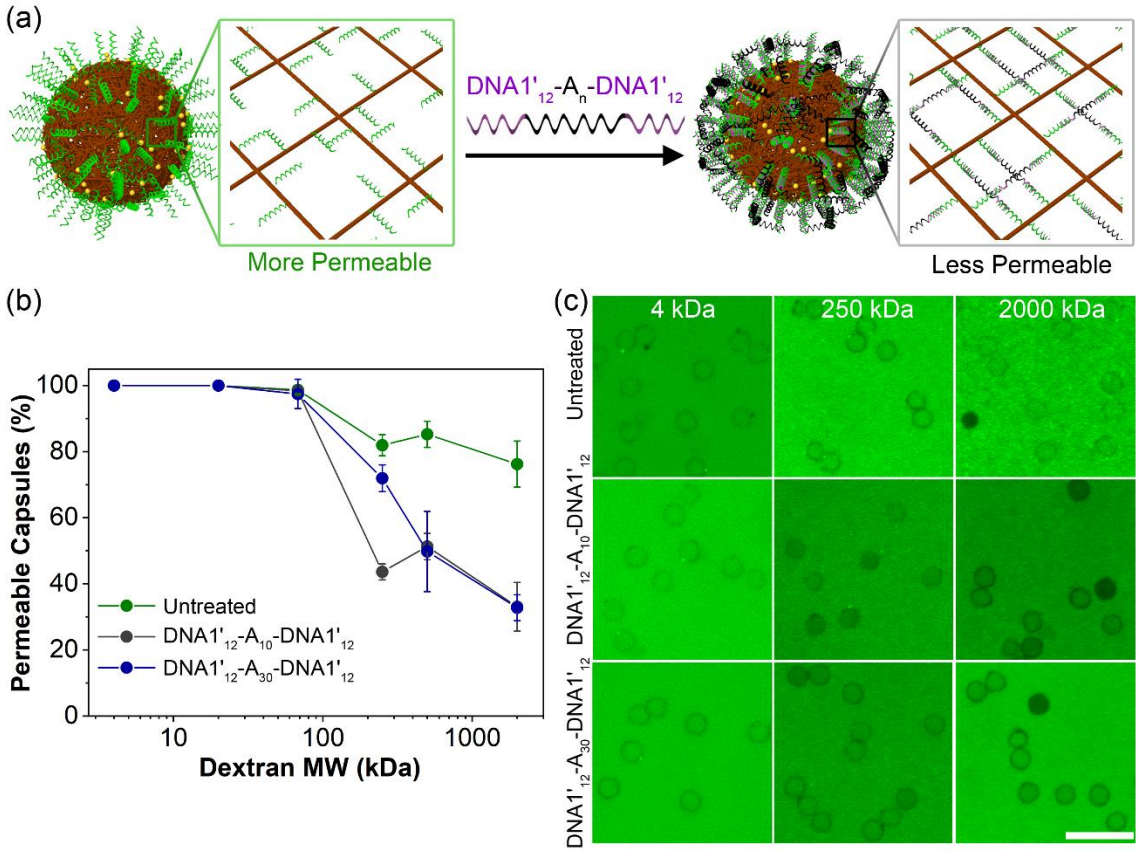

Figure 4. (a) Schematic illustration of permeability control of the DBC–Fe^{III} MPN capsules via hybridization with connector strands (DNA1′$_{12}$-A$_n$-DNA1′$_{12}$). (b) Permeability of DBC–Fe^{III} MPN capsules (3.25 μm) to FITC-dextran with molecular weight (MW) ranging from 4 to 2000 kDa, and corresponding representative confocal microscopy images (scale bar is 10 μm). The

permeability data are shown as the mean ± standard deviation for three independent experiments; 50–100 capsules were examined.

Cellular Uptake of DBC–Fe^{III} MPN Particles. Studies have shown that DNA-functionalized particles display efficient cellular uptake without the use of additional transfection reagents due to the high DNA density on particle surfaces.[26,28,60] We hypothesized that the DBC–Fe^{III} MPN particles would have similar uptake properties due to the densely packed oligonucleotides on the particle surface. Single-stranded DNA1(FAM) (i.e., ssDNA) and DBC–Fe^{III} MPN particles of different sizes (prepared using 0.147, 0.782, and 3.25 μm PS templates) were incubated with HeLa cells at a 10 nM DNA1(FAM) concentration for 24 h at 37 °C (Figure 5a), and the uptake was measured by flow cytometry. ssDNA showed negligible uptake due to the strong electrostatic repulsion between DNA and the negatively charged cell membrane.[8] In contrast, cellular uptake of the DBC–Fe^{III} MPN particles increased as particle size decreased (Figure 5a), with the average RFI increasing from 3.4 to 4.9 and 7.8 as particle size decreased from 3.25 to 0.782 and 0.147 μm. ζ-Potential measurements showed that the 0.147 μm particles were more negatively charged than the larger particles (ζ-potential values of −36.5 ± 0.7 mV, −27.2 ± 0.7 mV, and −11.8 ± 2.6 mV for the 0.147, 0.782, and 3.25 μm particles, respectively), indicating that the smaller particles have more densely packed DNA strands on the surface.[26] We note that our DBC–Fe^{III} MPN particles show comparable cellular uptake properties at a relatively low concentration (10 nM) to other reported DBC micelles that use higher concentrations of 200 nM[26] and 1 μM,[61] suggesting the potential of our particles as efficient delivery systems. To visualize particle uptake, the cell nucleus and membrane were stained using Hoechst 33342 (blue) and WGA594 (red), respectively, which do not overlap with the fluorescence from the MPN particles (green). In agreement with the flow cytometry results, the 0.147 μm DBC–Fe^{III} MPN particles, which were the smallest particles in the

present study, showed the most efficient cellular uptake results, as measured by CLSM. Therefore, the 0.147 μm DBC–Fe^{III} MPN particles were used in subsequent studies. Three different DBC–Fe^{III} MPN particles with different DNA surface densities were prepared by controlling the template particle concentration during assembly. The calculated DNA densities on the DBC–Fe^{III} MPN particle surfaces were 9.75×10^{12}, 2.92×10^{12}, and 1.88×10^{12} strands cm^{-2} (Table S3), which are comparable to those of previously reported DNA-functionalized particle systems.[26,53] These particles were denoted as high density (ρ), medium ρ, and low ρ in Figure 5b, respectively. Increasing the surface density of oligonucleotides resulted in enhanced cellular uptake, which demonstrates the importance of high DNA surface density for efficient cell internalization of MPN particles. This dependence of cellular uptake on DNA surface density was also reported for DNA block copolymer micelles and is considered to originate from the enhanced interactions between oligonucleotide strands at higher DNA density and receptors present on the cell surface.[26,61,62] The effects of incubation time (from 1 to 24 h) and particle concentration (equivalent to 0.5–10 nM DNA) on cellular uptake were also investigated (Figure S17). As expected, prolonged incubation and higher particle concentration generally resulted in increased particle internalization.

Enhancing the stability of DNA strands against nuclease-catalyzed hydrolysis is important for biomedical applications of therapeutic nucleic acids.[48] To investigate whether incorporating DNA strands into DBC–Fe^{III} MPN particles confers any protective effect, the DNA1(FAM) strands on the particle surface were pre-hybridized with DNA1′(Cy3) and subjected to nuclease-catalyzed degradation. Upon addition of deoxyribonuclease I (DNase I), the fluorescence intensity of FAM increased over time, indicating DNA degradation and release of FAM-labeled DNA fragments, as expected (Figure 5c). Compared to free ssDNA, the DBC–Fe^{III} MPN particles demonstrated

enhanced nucleic acid stability to DNase I, which is likely due to the dense oligonucleotide strands on the particle surface.[17]

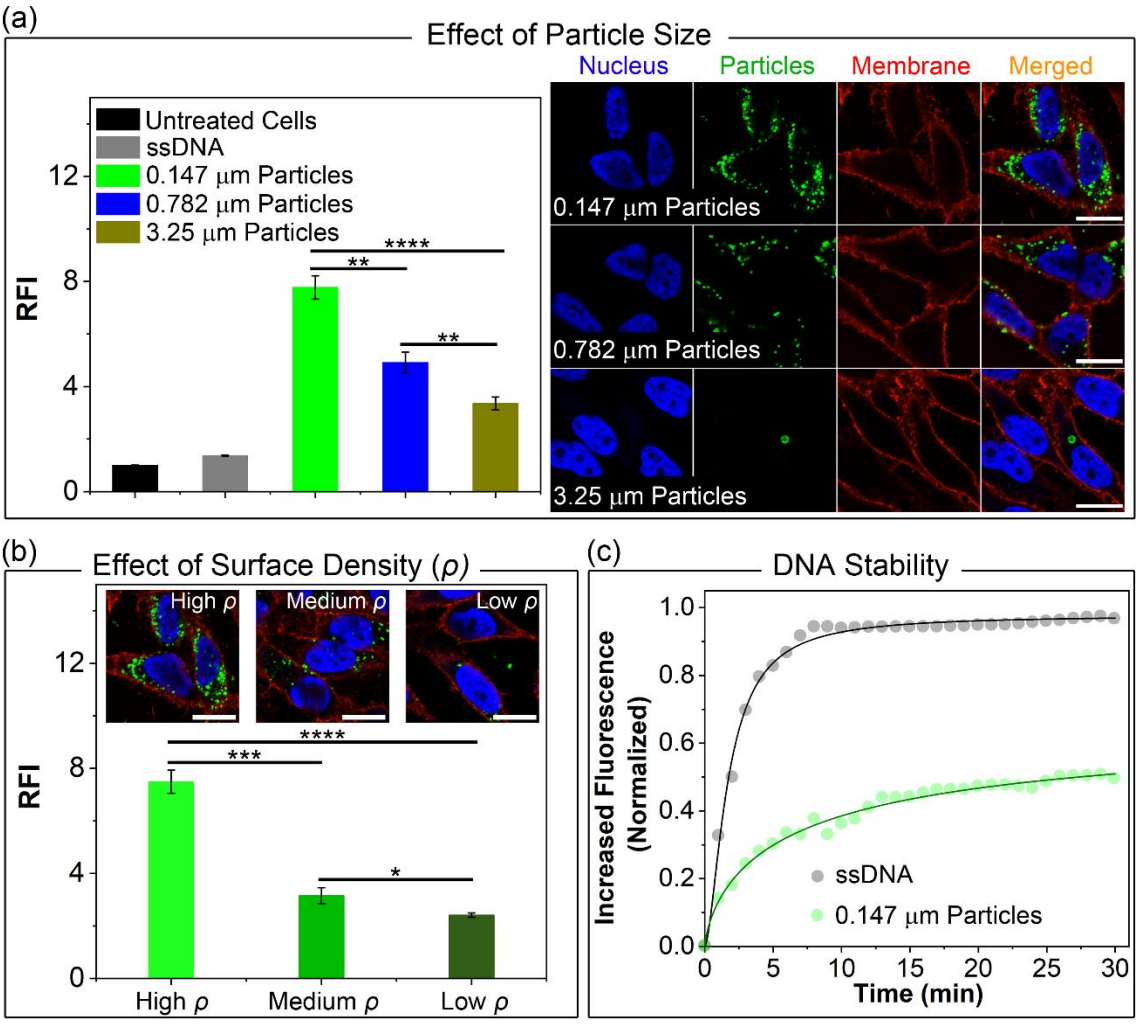

Figure 5. Cellular uptake properties of DBC–Fe^{III} MPN particles and enhanced stability of DNA strands in particles. Effects of (a) particle size and (b) surface density of 0.147 μm DBC–Fe^{III} MPN particles on intracellular uptake, as assessed by flow cytometry. HeLa cells were treated with DBC–Fe^{III} MPN particles (0.147, 0.782, or 3.25 μm) for 24 h at 37 °C. The concentration of the DBC–Fe^{III} MPN particles was 10 nM calculated based on the DNA concentration. The RFI to untreated cells is shown. Error bars represent the standard deviation of three independent experiments. Statistical significance was determined by one-way ANOVA: **** $p < 0.0001$, ***

$p < 0.001$, ** $p < 0.01$, and * $p < 0.05$. CLSM images of HeLa cells incubated with DBC–Fe^{III} particles for 24 h at 37 °C. Cell membranes and nuclei were stained with WGA594 (red) and Hoechst 33342 (blue), respectively. Green fluorescence represents DBC–Fe^{III} particles. (c) Nuclease-catalyzed degradation of DNA in ssDNA and 0.147 μm DBC–Fe^{III} particles at 25 °C.

For successful cytosolic delivery of therapeutic cargos, it is necessary to develop delivery systems that can escape from early/late endosomes before lysosomal degradation.[8,63] To investigate the endosomal escape capabilities of the DBC–Fe^{III} MPN particles (0.147 μm), colocalization analysis of the MPN particles with endo/lysosomes in HeLa cells was conducted (Figure S18). The cell nucleus was stained with Hoechst 33342 (blue) and endo/lysosomes with LysoTracker Red (red), neither of which overlapped with the fluorescence from the MPN particles (green). After incubation for 24 h, the DBC–Fe^{III} MPN particles displayed a low degree of colocalization with endo/lysosomes (Pearson's correlation coefficient (PCC) = 0.38 ± 0.07), suggesting that these particles escaped from endo/lysosomal compartments into the cytoplasm.[64] This result is likely due to the "proton-sponge effect" arising from the buffering capacity of coordination networks between the catechol groups in the DNA block copolymer chains and Fe^{III} ions.[64,65] These results demonstrate that the DBC–Fe^{III} MPN particles are potential candidates for the efficient delivery of therapeutic molecules.

Intracellular Trafficking, Uptake Mechanism, and siRNA Delivery of DBC–Fe^{III} MPN Particles. To further explore the intracellular trafficking of DBC–Fe^{III} MPN particles (0.147 μm) in HeLa cells, protein markers EEA1, Rab7, and LAMP1 were used to label early endosomal,[66] late endosomal,[67] and lysosomal[68] compartments, respectively. The DBC–Fe^{III} MPN particles emitted green fluorescence, which was derived from DNA1(FAM), whereas the cell nucleus was stained with Hoechst 33342 (blue) and the various cell compartments with the corresponding

monoclonal antibodies were labeled with Alexa Fluor 647 (Figure 6a). Colocalization between the particles and early/late endosomes remained low after both 12 and 24 h incubation, which suggests endosomal escape is achieved using these particles. Appreciable colocalization was not observed between the fluorescence signal arising from the particles and the lysosomal marker (LAMP-1) over the entire incubation period of 24 h, confirming that the DBC–Fe^{III} MPN particles do not progress through the typical endo-lysosomal pathway.

The endocytic pathways involved in the uptake of the DBC–Fe^{III} MPN particles (0.147 μm) were investigated to understand how these particles are internalized by cells (Figure 6b). Specific pathways of interest include macropinocytosis, and clathrin- and caveolae-mediated endocytosis.[8,69] Metabolic inhibitors EIPA, pitstop 2, and filipin from *S. filipinensis* were chosen for inhibiting macropinocytosis, and clathrin- and caveolae-dependent endocytosis, respectively.[70] HeLa cells were cultured with the endocytosis inhibitors for 15 min before adding the DBC–Fe^{III} MPN particles and then incubated with the particles for a further 24 h (Figure 6b). The particle uptake was not inhibited by pitstop 2, indicating that the clathrin-mediated uptake is not a significant contributor to endocytosis. In contrast, both EIPA and filipin reduced the uptake of particles by 39.7% and 33.0%, respectively, suggesting that the mechanism of cellular internalization of DBC–Fe^{III} MPN particles is likely a combination of macropinocytosis and caveolae-mediated endocytosis.[70]

The delivery of therapeutic oligonucleotides to target cells has been broadly used for selective gene silencing in biomedical research and disease treatment.[71,72] To evaluate the DBC–Fe^{III} MPN particles as a delivery system for a therapeutic oligonucleotide, luciferase siRNA conjugated to the DNA1 complementary DNA sequence (DNA1′$_{18}$-siRNA) was designed. The siRNA-functionalized DBC–Fe^{III} MPN particles were fabricated through the well-defined complementary

hybridization between DNA1 and DNA1′ (Figure 6c). DLS data showed an increase in hydrodynamic diameter (Figure 6d) when $DNA1'_{18}$-siRNA strands were mixed with the DBC–Fe^{III} MPN particles due to the hybridization of complementary sequences, indicating successful therapeutic particle formation. For the siRNA-regulated gene knockdown study, PC3-Luc2 cells were used. The introduction of siRNA-functionalized particles into the cells results in luciferase gene silencing, which can be detected from the luminescence intensity of luciferase-catalyzed luciferin[73] (Figure 6c). Gene silencing was detected through a luminescence assay at different time points. Specifically, 89% of protein expression was reduced by siRNA-functionalized DBC–Fe^{III} MPN particles up to 96 h after transfection, which is comparable to that achieved by siRNA complexed with commercial transfection agent (i.e., lipofectamine RNAiMax) (Figure 6d). As expected, there was no detectable gene silencing from free siRNA strands. Furthermore, the DBC–Fe^{III} MPN particles showed negligible cytotoxicity, suggesting their potential in biomedical and environmental applications (Figure S19). Altogether, the DBC–Fe^{III} MPN particles displayed efficient cellular uptake, endosomal escape and intracellular trafficking. Furthermore, the endocytic mechanism was successfully elucidated. We also demonstrated the efficient delivery of siRNA using these particles to achieve a reduction in a specific gene in model cells. These results indicate that DBC–Fe^{III} MPN particle systems may be promising delivery vehicles for therapeutic nucleic acids.

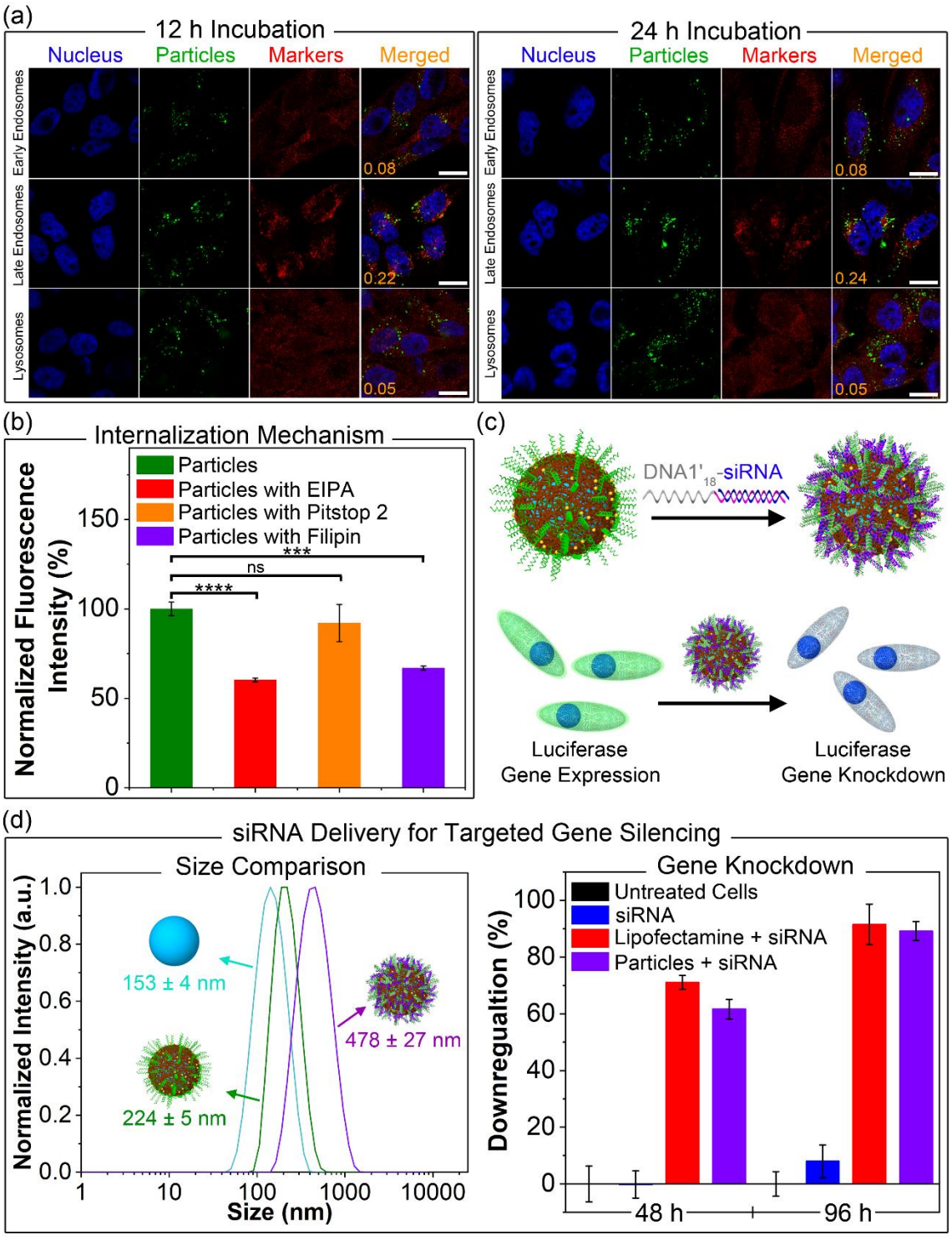

Figure 6. (a) CLSM images of HeLa cells incubated with 0.147 μm DBC–Fe^{III} MPN particles (green) for 12 or 24 h at 37 °C. Cell nuclei were stained with Hoechst 33342 (blue). Cell compartments (red) were stained with EEA1 monoclonal antibody (early endosome), anti-Rab7

monoclonal antibody (late endosome), or anti-LAMP1 monoclonal antibody (lysosome). PCC values are displayed in the "Merged" images. Scale bars are 20 μm. (b) Flow cytometry analysis of HeLa cells treated with 0.147 μm DBC–Fe^{III} MPN particles with endocytic inhibitors (i.e., pitstop 2, filipin, and EIPA) for 24 h at 37 °C. Statistical significance was determined by one-way ANOVA: **** $p < 0.0001$, *** $p < 0.001$ and ns not significantly different. The DNA concentration was 10 nM in the DBC–Fe^{III} MPN particles. The RFI to untreated cells is shown. Error bars represent the standard deviation of three independent experiments. (c) Schematic illustration of the preparation of siRNA-functionalized DBC–Fe^{III} MPN particles through DNA hybridization (top) and gene regulation in cells using these particles (bottom). (d) DLS size measurements of PS template particles (cyan), DBC–Fe^{III} MPN particles (green), and siRNA-functionalized DBC–Fe^{III} MPN particles (violet) in 25 mM MOPS (pH 7.4) solution containing 0.1 M NaCl. Hydrodynamic diameters are shown as the mean ± standard deviation of three measurements. Luciferase gene knockdown in PC3-Luc2 cells after 48 and 96 h transfections.

CONCLUSIONS

A DNA block copolymer (i.e., DNA-*b*-poly(MMA-*co*-DHCAF), which integrates hydrophobic blocks, catechol-containing blocks, and molecular recognition properties, was synthesized and applied as an MPN building block to prepare DNA-functionalized MPN particles and capsules. The MPN systems were fabricated on the basis of coordination networks formed between the catechol groups and Fe^{III} ions. Hydrogen bonding and hydrophobic interactions also contributed to the self-assembly of the MPNs. The resulting MPN systems showed high stability in various solutions containing strong acids, metal chelates, and surfactants. The specific molecular recognition properties of the DNA strands in the DBC–Fe^{III} MPN systems were preserved, enabling control of interactions with functional molecules and nanoparticles, and allowing

permeability tuning of the capsules. The DBC–Fe^{III} MPN particles exhibited efficient cellular uptake, with the smallest particles (0.147 μm) that featured the highest DNA surface density demonstrating the highest uptake. The enhanced oligonucleotide stability against nuclease-catalyzed hydrolysis and the endosomal escape capabilities of the DBC–Fe^{III} MPN particles make them promising candidates for intracellular nucleic acid delivery. Detailed intracellular trafficking and cellular uptake mechanism studies demonstrated that these particles undergo endosomal escape after internalization via a combination of macropinocytosis and caveolae-mediated endocytosis. Moreover, these particles efficiently delivered siRNA for specific gene knockdown in the cell. We anticipate that these DNA-functionalized particle and capsule systems may be useful for further materials and biomedical studies and have potential in various applications.

ASSOCIATED CONTENT

Supporting Information. Materials and instrumentation; synthesis of iBocDHCA, iBocDHCA methacrylate, poly(MMA_{40}-*co*-iBocDHCAF_{23}), DNA1(FAM)-*b*-poly(MMA_{40}-*co*-DHCAF_{23}); NMR, gel permeation chromatography, gel electrophoresis, DLS, UV–vis spectroscopy, DIC, SEM, TEM, AFM data; molecular dynamics simulation methods; additional in situ hybridization of DBC–Fe^{III} MPN capsules; additional permeability control data; additional intracellular uptake data; cytotoxicity data; MIRIBEL checklist for reporting research in bio–nano science. This material is available free of charge via the Internet at http://pubs.acs.org.

AUTHOR INFORMATION

Corresponding Author

*E-mail: fcaruso@unimelb.edu.au (F.C.)

Author Contributions

The manuscript was written through contributions of all authors. All authors have given approval to the final version of the manuscript.

Notes

The authors declare no competing financial interest.

ACKNOWLEDGMENT

This research was funded by the Australian Research Council (ARC) through the Discovery Project (DP200100713) scheme. F.C. acknowledges the award of a National Health and Medical Research Council Senior Principal Research Fellowship (GNT1135806). J.F.Q. acknowledges receipt of a Future Fellowship (FT170100144) from the ARC. This work was performed in part at the Materials Characterisation and Fabrication Platform (MCFP) at The University of Melbourne and the Victorian Node of the Australian National Fabrication Facility (ANFF). This research was supported by The University of Melbourne's Research Computing Services and the Petascale Campus Initiative. We thank Dr. Christina Cortez-Jugo, Dr. Francesca Cavalieri, Dr. Robert De Rose, and Denzil Furtado for helpful discussions.

REFERENCES

(1) Ejima, H.; Richardson, J. J.; Liang, K.; Best, J. P.; van Koeverden, M. P.; Such, G. K.; Cui, J.; Caruso, F. One-Step Assembly of Coordination Complexes for Versatile Film and Particle Engineering. *Science* **2013**, *341*, 154–157.

(2) Caruso, F.; Caruso, R. A.; Möhwald, H. Nanoengineering of Inorganic and Hybrid Hollow Spheres by Colloidal Templating. *Science* **1998**, *282*, 1111–1114.

(3) Zhou, J.; Creyer, M. N.; Chen, A.; Yim, W.; Lafleur, R. P. M.; He, T.; Lin, Z.; Xu, M.; Abbasi, P.; Wu, J., et al. Stereoselective Growth of Small Molecule Patches on Nanoparticles. *J. Am. Chem. Soc.* **2021**, *143*, 12138–12144.

(4) Mirkin, C. A.; Letsinger, R. L.; Mucic, R. C.; Storhoff, J. J. A DNA-Based Method for Rationally Assembling Nanoparticles into Macroscopic Materials. *Nature* **1996**, *382*, 607–609.

(5) Mai, Y.; Eisenberg, A. Self-Assembly of Block Copolymers. *Chem. Soc. Rev.* **2012**, *41*, 5969–5985.

(6) McMillan, J. R.; Hayes, O. G.; Winegar, P. H.; Mirkin, C. A. Protein Materials Engineering with DNA. *Acc. Chem. Res.* **2019**, *52*, 1939–1948.

(7) Blum, A. P.; Kammeyer, J. K.; Rush, A. M.; Callmann, C. E.; Hahn, M. E.; Gianneschi, N. C. Stimuli-Responsive Nanomaterials for Biomedical Applications. *J. Am. Chem. Soc.* **2015**, *137*, 2140–2154.

(8) Hu, Q.; Li, H.; Wang, L.; Gu, H.; Fan, C. DNA Nanotechnology-Enabled Drug Delivery Systems. *Chem. Rev.* **2019**, *119*, 6459–6506.

(9) Zhou, J.; Lin, Z.; Ju, Y.; Rahim, M. A.; Richardson, J. J.; Caruso, F. Polyphenol-Mediated Assembly for Particle Engineering. *Acc. Chem. Res.* **2020**, *53*, 1269–1278.

(10) Richardson, J. J.; Björnmalm, M.; Caruso, F. Technology-Driven Layer-by-Layer Assembly of Nanofilms. *Science* **2015**, *348*, 411.

(11) Guo, J.; Tardy, B. L.; Christofferson, A. J.; Dai, Y.; Richardson, J. J.; Zhu, W.; Hu, M.; Ju, Y.; Cui, J.; Dagastine, R. R., et al. Modular Assembly of Superstructures from Polyphenol-Functionalized Building Blocks. *Nat. Nanotechnol.* **2016**, *11*, 1105–1111.

(12) Kim, C.-J.; Ercole, F.; Ju, Y.; Pan, S.; Chen, J.; Qu, Y.; Quinn, J. F.; Caruso, F. Synthesis of Customizable Macromolecular Conjugates as Building Blocks for Engineering Metal–Phenolic Network Capsules with Tailorable Properties. *Chem. Mater.* **2021**, *33*, 8477–8488.

(13) Kim, C.-J.; Ercole, F.; Chen, J.; Pan, S.; Ju, Y.; Quinn, J. F.; Caruso, F. Macromolecular Engineering of Thermoresponsive Metal–Phenolic Networks. *J. Am. Chem. Soc.* **2022**, *144*, 503–514.

(14) Pan, S.; Guo, R.; Bertleff-Zieschang, N.; Li, S.; Besford, Q. A.; Zhong, Q.-Z.; Yun, G.; Zhang, Y.; Cavalieri, F.; Ju, Y., et al. Modular Assembly of Host–Guest Metal–Phenolic Networks Using Macrocyclic Building Blocks. *Angew. Chem. Int. Ed.* **2020**, *59*, 275–280.

(15) Whitfield, C. J.; Zhang, M.; Winterwerber, P.; Wu, Y.; Ng, D. Y. W.; Weil, T. Functional DNA–Polymer Conjugates. *Chem. Rev.* **2021**, *121*, 11030–11084.

(16) Seeman, N. C.; Sleiman, H. F. DNA Nanotechnology. *Nat. Rev. Mater.* **2017**, *3*, 17068.

(17) Cutler, J. I.; Auyeung, E.; Mirkin, C. A. Spherical Nucleic Acids. *J. Am. Chem. Soc.* **2012**, *134*, 1376–1391.

(18) Sun, H.; Yang, L.; Thompson, M. P.; Schara, S.; Cao, W.; Choi, W.; Hu, Z.; Zang, N.; Tan, W.; Gianneschi, N. C. Recent Advances in Amphiphilic Polymer–Oligonucleotide Nanomaterials Via Living/Controlled Polymerization Technologies. *Bioconjugate Chem.* **2019**, *30*, 1889–1904.

(19) Schnitzler, T.; Herrmann, A. DNA Block Copolymers: Functional Materials for Nanoscience and Biomedicine. *Acc. Chem. Res.* **2012**, *45*, 1419–1430.

(20) Kwak, M.; Herrmann, A. Nucleic Acid/Organic Polymer Hybrid Materials: Synthesis, Superstructures, and Applications. *Angew. Chem. Int. Ed.* **2010**, *49*, 8574–8587.

(21) Alemdaroglu, F. E.; Herrmann, A. DNA Meets Synthetic Polymers—Highly Versatile Hybrid Materials. *Org. Biomol. Chem.* **2007**, *5*, 1311–1320.

(22) Wilks, T. R.; Bath, J.; de Vries, J. W.; Raymond, J. E.; Herrmann, A.; Turberfield, A. J.; O'Reilly, R. K. "Giant Surfactants" Created by the Fast and Efficient Functionalization of a DNA Tetrahedron with a Temperature-Responsive Polymer. *ACS Nano* **2013**, *7*, 8561–8572.

(23) Jia, F.; Li, H.; Chen, R.; Zhang, K. Self-Assembly of DNA-Containing Copolymers. *Bioconjugate Chem.* **2019**, *30*, 1880–1888.

(24) Lueckerath, T.; Strauch, T.; Koynov, K.; Barner-Kowollik, C.; Ng, D. Y.; Weil, T. DNA–Polymer Conjugates by Photoinduced Raft Polymerization. *Biomacromolecules* **2018**, *20*, 212–221.

(25) Li, Z.; Zhang, Y.; Fullhart, P.; Mirkin, C. A. Reversible and Chemically Programmable Micelle Assembly with DNA Block-Copolymer Amphiphiles. *Nano Lett.* **2004**, *4*, 1055–1058.

(26) Kim, C.-J.; Kim, G.-H.; Jeong, E. H.; Lee, H.; Park, S.-J. The Core Composition of DNA Block Copolymer Micelles Dictates DNA Hybridization Properties, Nuclease Stabilities, and Cellular Uptake Efficiencies. *Nanoscale* **2021**, *13*, 13758–13763.

(27) Tan, X.; Lu, X.; Jia, F.; Liu, X.; Sun, Y.; Logan, J. K.; Zhang, K. Blurring the Role of Oligonucleotides: Spherical Nucleic Acids as a Drug Delivery Vehicle. *J. Am. Chem. Soc.* **2016**, *138*, 10834–10837.

(28) Rush, A. M.; Nelles, D. A.; Blum, A. P.; Barnhill, S. A.; Tatro, E. T.; Yeo, G. W.; Gianneschi, N. C. Intracellular mRNA Regulation with Self-Assembled Locked Nucleic Acid Polymer Nanoparticles. *J. Am. Chem. Soc.* **2014**, *136*, 7615–7618.

(29) Rush, A. M.; Thompson, M. P.; Tatro, E. T.; Gianneschi, N. C. Nuclease-Resistant DNA Via High-Density Packing in Polymeric Micellar Nanoparticle Coronas. *ACS Nano* **2013**, *7*, 1379–1387.

(30) Xiao, F.; Lin, L.; Chao, Z.; Shao, C.; Chen, Z.; Wei, Z.; Lu, J.; Huang, Y.; Li, L.; Liu, Q. Organic Spherical Nucleic Acids for the Transport of a NIR-II-Emitting Dye across the Blood–Brain Barrier. *Angew. Chem. Int. Ed.* **2020**, *59*, 9702–9710.

(31) Zheng, M.; Jiang, T.; Yang, W.; Zou, Y.; Wu, H.; Liu, X.; Zhu, F.; Qian, R.; Ling, D.; McDonald, K. The siRNAsome: A Cation-Free and Versatile Nanostructure for siRNA and Drug Co-Delivery. *Angew. Chem. Int. Ed.* **2019**, *131*, 4992–4996.

(32) Chien, M. P.; Rush, A. M.; Thompson, M. P.; Gianneschi, N. C. Programmable Shape-Shifting Micelles. *Angew. Chem. Int. Ed.* **2010**, *49*, 5076–5080.

(33) Kim, C.-J.; Hu, X.; Park, S.-J. Multimodal Shape Transformation of Dual-Responsive DNA Block Copolymers. *J. Am. Chem. Soc.* **2016**, *138*, 14941–14947.

(34) Kamps, A. C.; Cativo, M. H. M.; Chen, X.-J.; Park, S.-J. Self-Assembly of DNA-Coupled Semiconducting Block Copolymers. *Macromolecules* **2014**, *47*, 3720–3726.

(35) Luo, Q.; Shi, Z.; Zhang, Y.; Chen, X. J.; Han, S. Y.; Baumgart, T.; Chenoweth, D. M.; Park, S.-J. DNA Island Formation on Binary Block Copolymer Vesicles. *J. Am. Chem. Soc.* **2016**, *138*, 10157–10162.

(36) Kim, C.-J.; Park, J.-e.; Hu, X.; Albert, S. K.; Park, S.-J. Peptide-Driven Shape Control of Low-Dimensional DNA Nanostructures. *ACS Nano* **2020**, *14*, 2276–2284.

(37) Lu, X.; Fu, H.; Shih, K. C.; Jia, F.; Sun, Y.; Wang, D.; Wang, Y.; Ekatan, S.; Nieh, M. P.; Lin, Y., et al. DNA-Mediated Step-Growth Polymerization of Bottlebrush Macromonomers. *J. Am. Chem. Soc.* **2020**, *142*, 10297–10301.

(38) Ding, K.; Alemdaroglu, F. E.; Börsch, M.; Berger, R.; Herrmann, A. Engineering the Structural Properties of DNA Block Copolymer Micelles by Molecular Recognition. *Angew. Chem. Int. Ed.* **2007**, *46*, 1172–1175.

(39) Faria, M.; Bjornmalm, M.; Thurecht, K. J.; Kent, S. J.; Parton, R. G.; Kavallaris, M.; Johnston, A. P. R.; Gooding, J. J.; Corrie, S. R.; Boyd, B. J., et al. Minimum Information Reporting in Bio–Nano Experimental Literature. *Nat. Nanotechnol.* **2018**, *13*, 777–785.

(40) Willcock, H.; O'Reilly, R. K. End Group Removal and Modification of Raft Polymers. *Polym. Chem.* **2010**, *1*, 149–157.

(41) Nakamura, K.; Nakajima, T.; Kayahara, H.; Nomura, E.; Taniguchi, H. Base-Labile *Tert*-Butoxycarbonyl (Boc) Group on Phenols. *Tetrahedron Lett.* **2004**, *45*, 495–499.

(42) Sagle, L. B.; Zhang, Y.; Litosh, V. A.; Chen, X.; Cho, Y.; Cremer, P. S. Investigating the Hydrogen-Bonding Model of Urea Denaturation. *J. Am. Chem. Soc.* **2009**, *131*, 9304–9310.

(43) Bam, N. B.; Cleland, J. L.; Randolph, T. W. Molten Globule Intermediate of Recombinant Human Growth Hormone: Stabilization with Surfactants. *Biotechnol. Prog.* **1996**, *12*, 801–809.

(44) Shim, T. S.; Estephan, Z. G.; Qian, Z.; Prosser, J. H.; Lee, S. Y.; Chenoweth, D. M.; Lee, D.; Park, S.-J.; Crocker, J. C. Shape Changing Thin Films Powered by DNA Hybridization. *Nat. Nanotechnol.* **2017**, *12*, 41–47.

(45) He, Y.; Ye, T.; Su, M.; Zhang, C.; Ribbe, A. E.; Jiang, W.; Mao, C. Hierarchical Self-Assembly of DNA into Symmetric Supramolecular Polyhedra. *Nature* **2008**, *452*, 198–201.

(46) Rothemund, P. W. Folding DNA to Create Nanoscale Shapes and Patterns. *Nature* **2006**, *440*, 297–302.

(47) Park, S.-J.; Taton, T. A.; Mirkin, C. A. Array-Based Electrical Detection of DNA with Nanoparticle Probes. *Science* **2002**, *295*, 1503–1506.

(48) Chandrasekaran, A. R. Nuclease Resistance of DNA Nanostructures. *Nat. Rev. Chem.* **2021**, *5*, 225–239.

(49) Sontakke, V. A.; Yokobayashi, Y. Programmable Macroscopic Self-Assembly of DNA-Decorated Hydrogels. *J. Am. Chem. Soc.* **2022**, *144*, 2149–2155.

(50) Rogers, W. B.; Manoharan, V. N. Programming Colloidal Phase Transitions with DNA Strand Displacement. *Science* **2015**, *347*, 639–642.

(51) Sebba, D. S.; Mock, J. J.; Smith, D. R.; LaBean, T. H.; Lazarides, A. A. Reconfigurable Core–Satellite Nanoassemblies as Molecularly-Driven Plasmonic Switches. *Nano Lett.* **2008**, *8*, 1803–1808.

(52) Storhoff, J. J.; Elghanian, R.; Mucic, R. C.; Mirkin, C. A.; Letsinger, R. L. One-Pot Colorimetric Differentiation of Polynucleotides with Single Base Imperfections Using Gold Nanoparticle Probes. *J. Am. Chem. Soc.* **1998**, *120*, 1959–1964.

(53) Hill, H. D.; Millstone, J. E.; Banholzer, M. J.; Mirkin, C. A. The Role Radius of Curvature Plays in Thiolated Oligonucleotide Loading on Gold Nanoparticles. *ACS Nano* **2009**, *3*, 418–424.

(54) Hanselmann, R.; Burchard, W.; Lemmes, R.; Schwengers, D. Characterization of DEAE-Dextran by Means of Light Scattering and Combined Size-Exclusion Chromatography/Low-Angle Laser Light Scattering/Viscometry. *Macromol. Chem. Phys.* **1995**, *196*, 2259–2275.

(55) Fragasso, A.; De Franceschi, N.; Stommer, P.; van der Sluis, E. O.; Dietz, H.; Dekker, C. Reconstitution of Ultrawide DNA Origami Pores in Liposomes for Transmembrane Transport of Macromolecules. *ACS Nano* **2021**, *15*, 12768–12779.

(56) Mura, S.; Nicolas, J.; Couvreur, P. Stimuli-Responsive Nanocarriers for Drug Delivery. *Nat. Mater.* **2013**, *12*, 991–1003.

(57) Liu, Z.; Wang, W.; Xie, R.; Ju, X.-J.; Chu, L.-Y. Stimuli-Responsive Smart Gating Membranes. *Chem. Soc. Rev.* **2016**, *45*, 460–475.

(58) Chandrawati, R.; Hosta-Rigau, L.; Vanderstraaten, D.; Lokuliyana, S. A.; Stadler, B.; Albericio, F.; Caruso, F. Engineering Advanced Capsosomes: Maximizing the Number of Subcompartments, Cargo Retention, and Temperature-Triggered Reaction. *ACS Nano* **2010**, *4*, 1351–1361.

(59) Park, H. B.; Kamcev, J.; Robeson, L. M.; Elimelech, M.; Freeman, B. D. Maximizing the Right Stuff: The Trade-Off between Membrane Permeability and Selectivity. *Science* **2017**, *356*, eaab0530.

(60) Wu, X. A.; Choi, C. H.; Zhang, C.; Hao, L.; Mirkin, C. A. Intracellular Fate of Spherical Nucleic Acid Nanoparticle Conjugates. *J. Am. Chem. Soc.* **2014**, *136*, 7726–7733.

(61) Zhang, C.; Hao, L.; Calabrese, C. M.; Zhou, Y.; Choi, C. H. J.; Xing, H.; Mirkin, C. A. Biodegradable DNA-Brush Block Copolymer Spherical Nucleic Acids Enable Transfection Agent-Free Intracellular Gene Regulation. *Small* **2015**, *11*, 5360–5368.

(62) Choi, C. H.; Hao, L.; Narayan, S. P.; Auyeung, E.; Mirkin, C. A. Mechanism for the Endocytosis of Spherical Nucleic Acid Nanoparticle Conjugates. *Proc. Natl. Acad. Sci. U. S. A.* **2013**, *110*, 7625–7630.

(63) Lee, J.; Sands, I.; Zhang, W.; Zhou, L.; Chen, Y. DNA-Inspired Nanomaterials for Enhanced Endosomal Escape. *Proc. Natl. Acad. Sci. U. S. A.* **2021**, *118*, e2104511118.

(64) Chen, J.; Li, J.; Zhou, J.; Lin, Z.; Cavalieri, F.; Czuba-Wojnilowicz, E.; Hu, Y.; Glab, A.; Ju, Y.; Richardson, J. J., et al. Metal–Phenolic Coatings as a Platform to Trigger Endosomal Escape of Nanoparticles. *ACS Nano* **2019**, *13*, 11653–11664.

(65) Chen, J.; Pan, S.; Zhou, J.; Seidel, R.; Beyer, S.; Lin, Z.; Richardson, J. J.; Caruso, F. Metal–Phenolic Networks as Tunable Buffering Systems. *Chem. Mater.* **2021**, *33*, 2557–2566.

(66) Mu, F.-T.; Callaghan, J. M.; Steele-Mortimer, O.; Stenmark, H.; Parton, R. G.; Campbell, P. L.; McCluskey, J.; Yeo, J.-P.; Tock, E. P.; Toh, B.-H. EEA1, an Early Endosome-Associated Protein. *J. Biol. Chem.* **1995**, *270*, 13503–13511.

(67) Chavrier, P.; Parton, R. G.; Hauri, H. P.; Simons, K.; Zerial, M. Localization of Low Molecular Weight GTP Binding Proteins to Exocytic and Endocytic Compartments. *Cell* **1990**, *62*, 317–329.

(68) Carlsson, S. R.; Fukuda, M. Structure of Human Lysosomal Membrane Glycoprotein 1: Assignment of Disulfide Bonds and Visualization of Its Domain Arrangement. *J. Biol. Chem.* **1989**, *264*, 20526–20531.

(69) Lee, D. S.; Qian, H.; Tay, C. Y.; Leong, D. T. Cellular Processing and Destinies of Artificial DNA Nanostructures. *Chem. Soc. Rev.* **2016**, *45*, 4199–4225.

(70) Wojnilowicz, M.; Glab, A.; Bertucci, A.; Caruso, F.; Cavalieri, F. Super-Resolution Imaging of Proton Sponge-Triggered Rupture of Endosomes and Cytosolic Release of Small Interfering RNA. *ACS Nano* **2019**, *13*, 187–202.

(71) Lee, H.; Lytton-Jean, A. K.; Chen, Y.; Love, K. T.; Park, A. I.; Karagiannis, E. D.; Sehgal, A.; Querbes, W.; Zurenko, C. S.; Jayaraman, M., et al. Molecularly Self-Assembled Nucleic Acid Nanoparticles for Targeted In Vivo siRNA Delivery. *Nat. Nanotechnol.* **2012**, *7*, 389–393.

(72) Whitehead, K. A.; Langer, R.; Anderson, D. G. Knocking Down Barriers: Advances in siRNA Delivery. *Nat. Rev. Drug Discovery* **2009**, *8*, 129–138.

(73) Chen, J.; Pan, S.; Zhou, J.; Lin, Z.; Qu, Y.; Glab, A.; Han, Y.; Richardson, J. J.; Caruso, F. Assembly of Bioactive Nanoparticles Via Metal–Phenolic Complexation. *Adv. Mater.* **2021**, *34*, 2108624.

Table of Contents Graphic (8.25 × 4.45 cm)